New Journal of Physics
The open access journal at the forefront of physics

Deutsche Physikalische Gesellschaft DPG IOP Institute of Physics

PAPER • OPEN ACCESS

Twinned-domain-induced magnonic modes in epitaxial LSMO/STO films

To cite this article: Erik Wahlström *et al* 2017 *New J. Phys.* **19** 063002

New Journal of Physics
The open access journal at the forefront of physics

Deutsche Physikalische Gesellschaft DPG
IOP Institute of Physics

Published in partnership with: Deutsche Physikalische Gesellschaft and the Institute of Physics

OPEN ACCESS

RECEIVED
14 February 2017

REVISED
20 April 2017

ACCEPTED FOR PUBLICATION
3 May 2017

PUBLISHED
2 June 2017

PAPER

Twinned-domain-induced magnonic modes in epitaxial LSMO/STO films

Erik Wahlström[1], Ferran Macià[2,7], Jos E Boschker[3,4], Åsmund Monsen[1], Per Nordblad[5], Roland Mathieu[5], Andrew D Kent[6] and Thomas Tybell[3]

[1] Department of Physics, NTNU, Norwegian Univ. of Science and Techn., 7491 Trondheim, Norway
[2] Institut de Ciència de Materials de Barcelona (ICMAB-CSIC), Campus UAB, E-08193 Bellaterra, Spain
[3] Department of Electronic systems, Norwegian Univ. of Science and Techn. 7491 Trondheim, Norway
[4] Leibniz Institute for Crystal Growth, Max-Born-Str. 2, D-12489 Berlin, Germany
[5] Department of Engineering Sciences, Uppsala University, Box 534, SE-751 21 Uppsala, Sweden
[6] Department of Physics, New York University, 4 Washington Place, New York, NY 10003, United States of America
[7] Author to whom any correspondence should be addressed.

E-mail: erik.wahlstrom@ntnu.no **and** fmacia@csic.es

Keywords: magnonics, epitaxial LSMO/STO films, FMR, twin domains

Abstract

The use of periodic magnetic structures to control the magneto-dynamic properties of materials—magnonics—is a rapidly developing field. In the last decade, a number of studies have shown that metallic films can be patterned or combined in patterns that give rise to well-defined magnetization modes, which are formed due to band folding or band gap effects. To explore and utilize these effects in a wide frequency range, it is necessary to pattern samples at the sub-micrometer scale. However, it is still a major challenge to produce low-loss magnonic structures with periodicities at such length scales. Here, we show that for a prototypical perovskite, $La_{0.7}$ $Sr_{0.3}$ MnO_3, the twinned structural order can be used to induce a magnetic modulation with a period smaller than 100 nm, demonstrating a bottom-up approach for magnonic crystal growth.

Use of the high-frequency resonances of magnetic materials has had a technological impact since the second world war, and has been dominated by the use of yttrium-iron-garnet in devices such as widely tunable oscillators and filters. These devices often rely on uniform excitation modes, characterized by a wave vector $\mathbf{q} = 0$. It is also possible to excite modes with $\mathbf{q} \neq 0$ associated with a periodic magnetic structure [1–4].

Such structures are denominated magnonic crystals and allow dynamic modes with different resonance frequencies to be established as well as the formation of frequency band gaps, offering the opportunity to build novel magnetic thin-film devices with well controllable properties [5]. Alternating a material with different magnetic properties was first proposed in order to create frequency band gaps in a magnetic film [6, 7]. A magnonic crystal is in general a magnetic metamaterial with magnetic properties that come from its geometrical structure rather than directly from its band structure or composition. Thus, it is necessary to define patterns on magnetic materials with periodicities at the relevant length scales associated with the magnetic energies responsible for dynamic-mode formation: basically, the magnetic exchange energy. Patterns with dimensions of tens of nanometer are required, usually demanding expensive and time-consuming lithography methods [6–12]. It is thus a major challenge to fabricate low-cost magnonic structures with periodicities of this small size.

Here, we show that twinned structural order in a perovskite with a composition of $La_{0.7}Sr_{0.3}$ MnO_3/$SrTiO_3$(001) (LSMO/STO) induced by crystal growth produces a modulation of the film magnetization with a period that is smaller than 100 nm, effectively creating a magnonic crystal. The LSMO thin films were grown by pulsed laser deposition (PLD) onto an STO substrate (details on sample fabrication and characterization are reported in [13]).

Perovskite-based magnetic systems are model systems in this regard, because their magnetic properties depend on the local structure of the material. In particular, it has been shown that there exist localized regions with a higher Curie temperature, T_C, in LSMO films [14–17]. In this article, we show that regions of enhanced

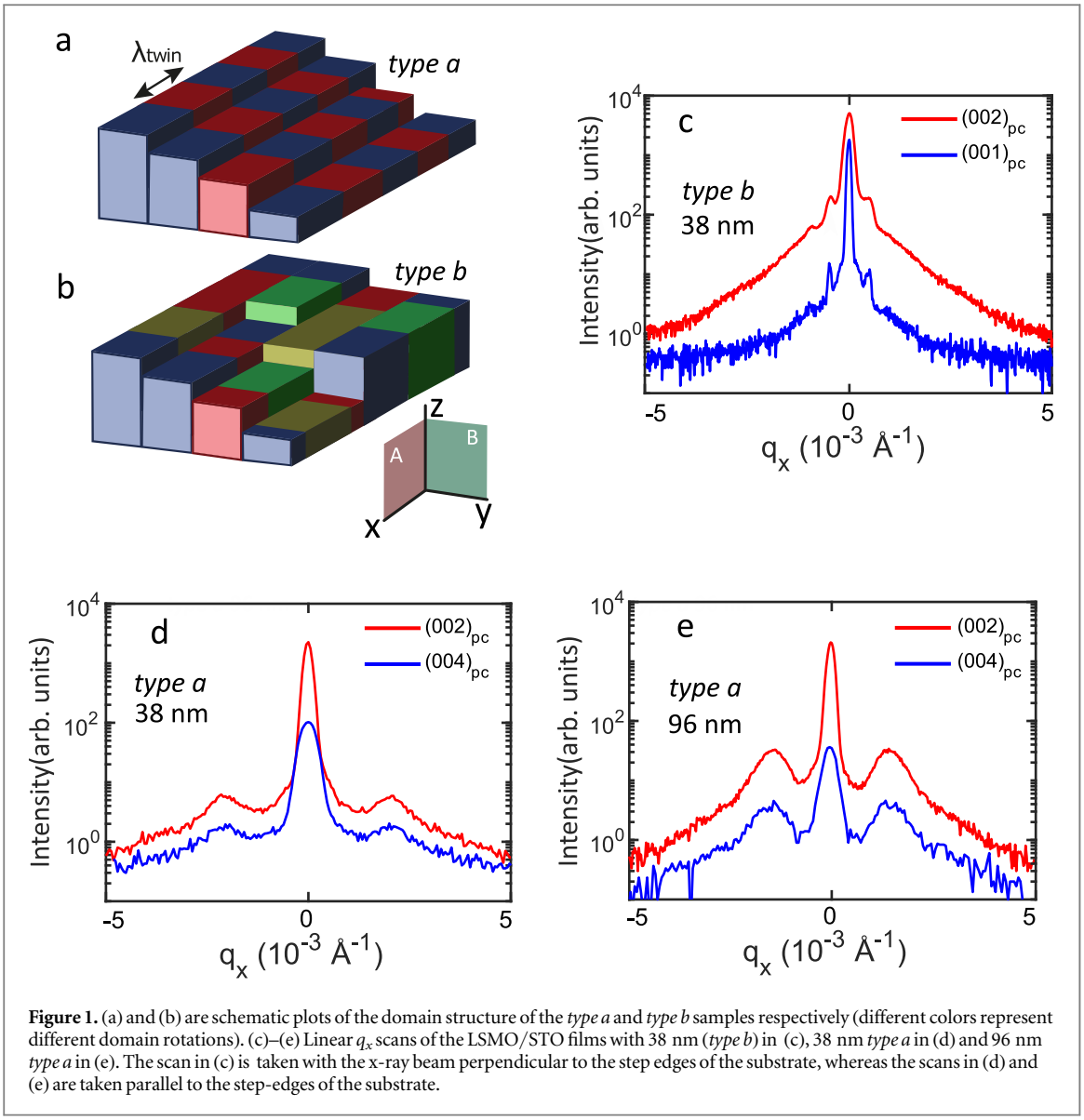

Figure 1. (a) and (b) are schematic plots of the domain structure of the *type a* and *type b* samples respectively (different colors represent different domain rotations). (c)–(e) Linear q_x scans of the LSMO/STO films with 38 nm (*type b*) in (c), 38 nm *type a* in (d) and 96 nm *type a* in (e). The scan in (c) is taken with the x-ray beam perpendicular to the step edges of the substrate, whereas the scans in (d) and (e) are taken parallel to the step-edges of the substrate.

T_C can be periodically introduced in an LSMO thin film and used to create a magnetization modulation that results in the appearance of short wave length spin-wave modes (or magnonic modes) of the system without using lithography techniques.

LSMO is the most widely studied of the manganese oxides due to its high Curie temperature (bulk $T_C \approx 370$ K), a high degree of spin polarization [18, 19], and the existence of the colossal magnetoresistive effect [20]. Prior investigations of LSMO thin films indicate that it has relatively low magnetodynamic damping [21–23], which is one of the prerequisites for use in devices. Bulk LSMO has a rhombohedral unit cell that slightly deviates from the cubic unit cell of the (001) surface of an STO substrate. This mismatch between the film and the substrate drives the formation of structural domains resulting in regions with different directions of rhombohedral distortion in the LSMO film. In total there are four possible orientations of LSMO with respect to the underlying substrate, and thus four possible variances are possible. It has been shown that both the number of orientations and the periodicity can be controlled by the vicinal cut of the substrate and the growth conditions [13]. Figures 1(a) and (b) schematically illustrate LSMO films on the STO with two different orientations (*type a*) and four different orientations (*type b*), respectively. In particular, for films grown with only two different orientations of LSMO (*type a*, figure 2(a)), it has been shown by Boschker *et al* [13] that the film forms spatially well-ordered domains with a twinned structure of periodicity, λ_{twin}, in one direction (x direction).

We studied samples of *type a* and *b* of LSMO with different thicknesses. The in-plane domain structure of the LSMO films is characterized by means of XRD. Figures 1(c)–(e) show the linear q_x scans of the three investigated samples with thicknesses of 38 nm (*type b*), 38 nm *type a* and 96 nm *type a* respectively. The latter two samples were grown on a substrate with a miscut of 0.5 degrees in the (100) direction. The scan in figure 1(c)

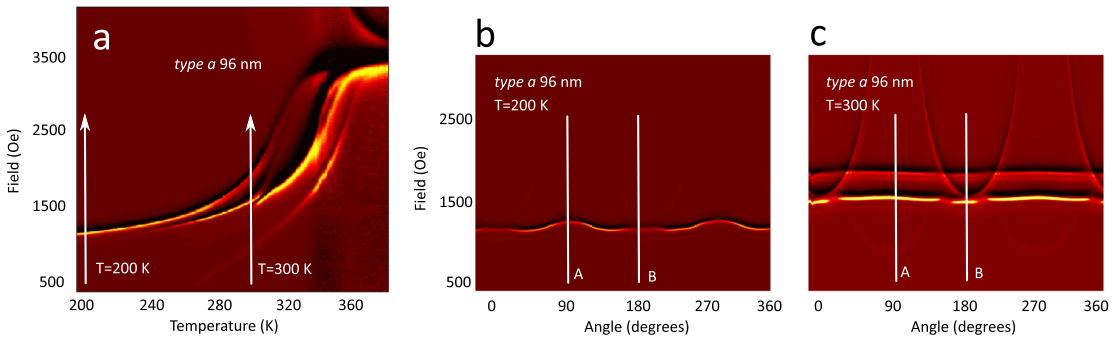

Figure 2. (a) The temperature dependence of the FMR spectra for a *type a* sample 96 nm thick with the field applied along the x direction (perpendicular to the twin domain boundaries). (b) Angular dependence of the FMR modes at 200 K, the vertical line marks the direction of planes A and B, described in the inset of the figure. (c) Angular dependence of the FMR modes at 300 K. The colors represent the differential adsorption data and are acquired at 9.37 GHz.

was taken with the x-ray beam approximately perpendicular to the step edges of the substrate. Clear satellite peaks can be seen on the left and right side of the main diffraction peaks. The satellite peaks occur at a constant separation in reciprocal space, indicating that they are due to an in-plane periodicity. From the separation between the satellite peaks and main reflection ($\Delta q_x = 5 \times 10^{-4}$ Å^{-1}) an in-plane periodicity of 200 nm is determined. This periodicity is coherent with the terrace width of the substrate in agreement with step-edge-induced structural distortions in the film [13]. We note that such distortions are typical for films with four variants. The presence of four variants is also confirmed by φ-scans around the $(022)_{pc}$ and $(202)_{pc}$ diffraction peaks.

The scans shown in panels (d) and (e) of figure 1 were taken with the x-ray beam parallel to the step-edges. Clear satellite peaks are also observed in this case, indicating a periodic in-plane structure. The separation between the satellite and main peak is substantially larger: 2.1×10^{-3} Å^{-1} and 1.4×10^{-3} Å^{-1} for the scans in (d) and (e), respectively. This corresponds to in-plane periodicities of 48 nm and 71 nm, respectively. These periodicities are probed with the x-ray beam parallel to the step-edges, and thus we can rule out the step-edges having caused the observed periodicity. Instead, we attribute the periodicity to the presence of periodic domains [13]. We note that such a periodicity was not observed when the x-ray beam was perpendicular to the step-edges, indicating that only two types of domain are present in the sample.

A periodic strain could cause a periodic variation of the Curie temperature, T_C, of the LSMO film [14–17], thus creating a modulation of the internal effective field caused by the different saturation magnetization values (especially at temperatures around the Curie temperature) and eventually introducing additional modes to the ferromagnetic resonance (FMR). To investigate this prediction, we first studied thick samples (96 nm) of two variants, *type a*, and found direct evidence of a splitting of the FMR mode with increasing temperature (i.e., when approaching the Curie temperature).

Figure 2(a) shows the temperature dependence of the FMR spectra on the magnetic field applied in the x direction, perpendicular to the twin domain boundaries. From this data we thus estimated Curie temperatures of $\simeq 370$ K and $\simeq 350$ K for the two modes of the film. Additional FMR spectra are presented in figures 2(b) and (c) showing the angular dependence of the external applied field in the sample plane at two different temperatures. At $T = 200$ K the two sample regions are still far from the Curie temperature and thus have a very similar magnetization value, presenting a single FMR peak (there is a small uniaxial anisotropy of the FMR mode). At $T = 300$ K the magnetization of the two sample regions has begun to change and the FMR mode has split into two modes (showing almost no uniaxial anisotropy). We notice that at $T = 300$ K there has appeared an additional weaker mode with a strong uniaxial anisotropy (with a preferred direction along the domain direction, the y direction) that was not visible in the temperature dependence shown in figure 2(a), and we may attribute this to a mode related to the domain walls (DWM).

To investigate the nature of these modes further, we acquired spectra at $T = 300$ K along the two planes perpendicular to the film, corresponding to directions with the biasing field perpendicular (plane A) and parallel (plane B) to the domain walls (figures 3(a)–(b)). We observe that the split FMR mode has a strong asymmetry when we rotate the angle in planes A and B indicating that the magnetization has in-plane anisotropy. We also observe that the main mode we attributed to the domain walls (DWM) has asymmetry when rotating the angle within plane A and it is rather symmetric when rotating in plane B.

We have selected substrates and parameters to obtain two new samples with magnetic modulation with an identical thickness (38 nm). These samples allow us to compare the magneto-dynamic modes: one is magnetically ordered, with a magnetic modulation, *type a*, (it is twinned with $\lambda_{twin} = 48$ nm modulation),

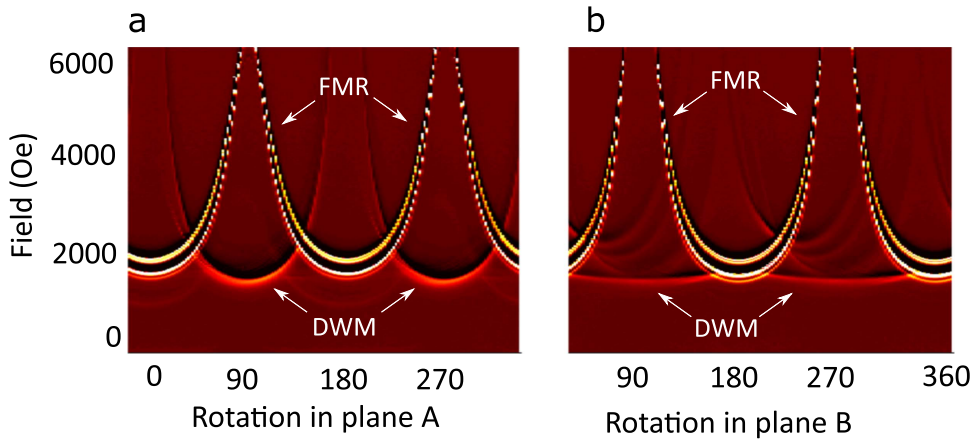

Figure 3. Rotational dependent FMR spectra acquired at $T = 300$ K in different rotational planes. (a) Rotation in plane A (plane perpendicular to the domain wall rotation); (b) rotation in plane B (plane parallel to the domain wall rotation).

whereas the other one is magnetically disordered, *type b*. The *type b* sample displays a weak step-edge-induced structural periodicity as measured by x-ray diffraction (XRD) [13]. Both samples display almost identical static magnetic properties, as indicated by the temperature-dependent saturation magnetization (figure 4(a)). At low temperatures both samples have a similar FMR response with a single FMR line, well described by the Kittel equations [24] at the given measured magnetization (dashed blue lines in figures 4(c) and (d)). However, at $\simeq$260 K an additional mode appears for the *type a* sample that crosses the main FMR mode at $\simeq$310 K. The mode crossing provides evidence that this is not an ordinary surface or volume mode, but a separate magnonic mode that has formed due to the modulation of the internal effective magnetic field. We also performed broadband FMR measurements with a coplanar waveguide to show that the additional mode behaves the same as the main mode. Figure 4(b) shows the measurement of the field dispersion in the *type a* sample at $T = 300$ K displaying the two resonance peaks. We argue in the following that the observed mode is a separate localized mode that has formed due to the modulation of the magnetic potential (i.e. the modulation of the internal effective magnetic field).

To describe and understand the origin of the possible coupling between the domain structure induced in the magnetic film and the magneto-dynamic modes , we used a model that accounts for the effective magnetization within the film. In the model we considered the modes as ordinary magneto-dynamic modes perturbed by the structural domain modulation of the magnetic potential. In general, a magnetic structure with a spatial periodic modulation, λ, introduces two new characteristic features in the FMR spectra (figure 5(a)): (i) the excitation of states with $q = 2\pi n/\lambda$, corresponding to a folding of the spin-wave band structure into the first Brillouin zone, and (ii) the opening of band gaps in the energy-wave vector relation. In the extreme case of fully localized waves (standing waves), only discrete states with a well-defined momentum $q = 2\pi n/\lambda$ can be excited.

In the studied system, these effects can be incorporated into an analytical model that describes the dynamic modes, limited to first order corrections due to exchange energies [24]. Effects due to band folding are found by modeling the system with the momentum, q_x, introduced by the periodic modulation length, λ_{twin}, while corrections for band gap formation are made through an estimation of the magnetic potential that stems from the spatial variation of the saturation magnetization. In the first case, we use a general description for the dispersion relations based on (*lmn*) indices, where the integers l, m and n yield the wave numbers in different directions: $q_z = \frac{2\pi n}{d}$, d is the film thickness and $q_x = \frac{2\pi l}{\lambda_{\text{twin}}}$:

$$\frac{\omega^2}{\gamma^2} = (H + D({q_z}^2 + {q_x}^2))\left(H + D({q_z}^2 + {q_x}^2) + \frac{4\pi M_{\text{eff}}}{1 + \frac{{q_z}^2}{{q_x}^2}}\right), \quad (1)$$

where D is the temperature-dependent spin wave stiffness obtained from the literature [21]. In the y-direction, $m = 0$ since this direction does not display structural periodicity. Thus, only variations in the directions of the twin boundaries, l, and the film thickness, n, are considered. In this model, any anisotropy can be incorporated into M_{eff}. The anisotropies of LSMO have been measured and found not to dominate the main mode analyzed here [22]; accordingly they have been neglected in this analysis.

Apart from the additional modes corresponding to the excited states, $q \neq 0$, we must understand the gap formation and evolution with temperature in the dispersion relation. In order to do this, we make a Fourier series expansion of the modulation of the effective magnetic potential at each temperature, starting with the base

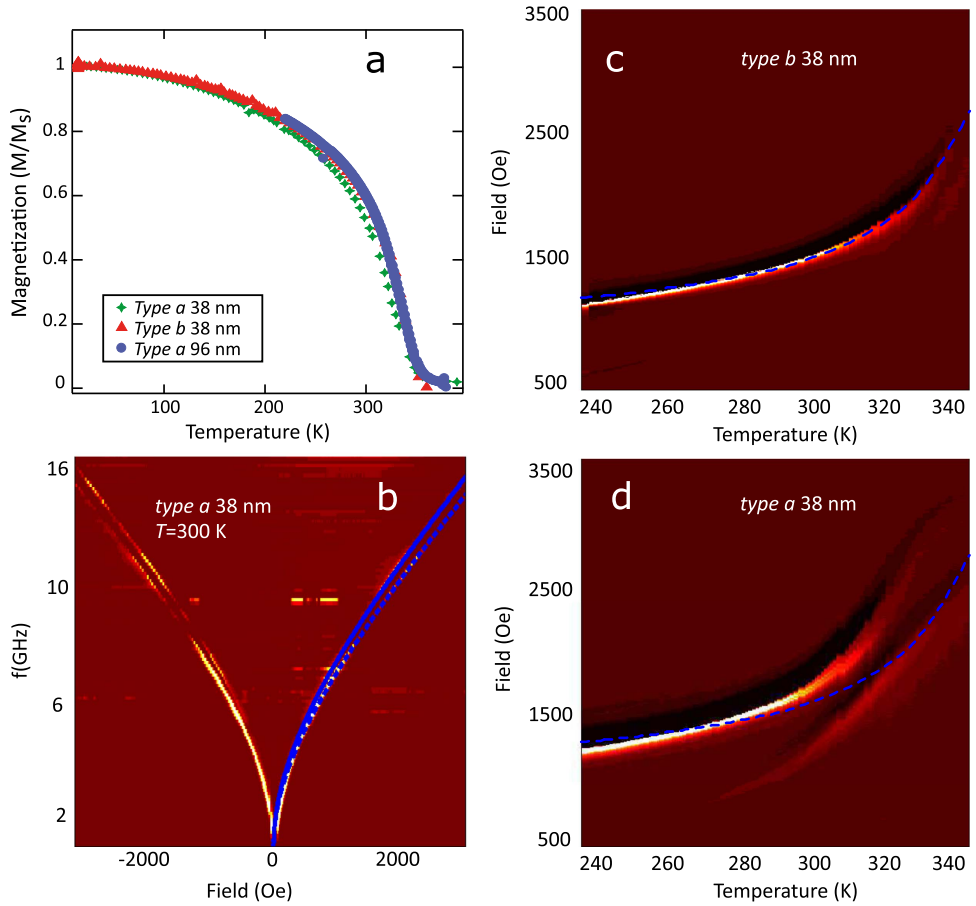

Figure 4. (a) The temperature dependence of the saturation magnetization of a 38 nm thick sample *type a* and two samples *type b* with thicknesses of 38 nm and 96 nm. (b) The in-plane measurement of the field dispersion FMR for the 38 nm thick *type a* sample at $T = 300$ K displaying two modes. The blue solid line corresponds to the model calculation for the FMR main peak and the dashed blue line corresponds to the calculation of the 101 mode. (c) and (d) show the temperature dependence of the 9.37 GHz FMR spectra of the 38 nm thick *type a* and *type b* samples respectively. The color scale corresponds to the differential adsorption amplitude, and the blue lines are fits to the uniform FMR mode, being the same in both images.

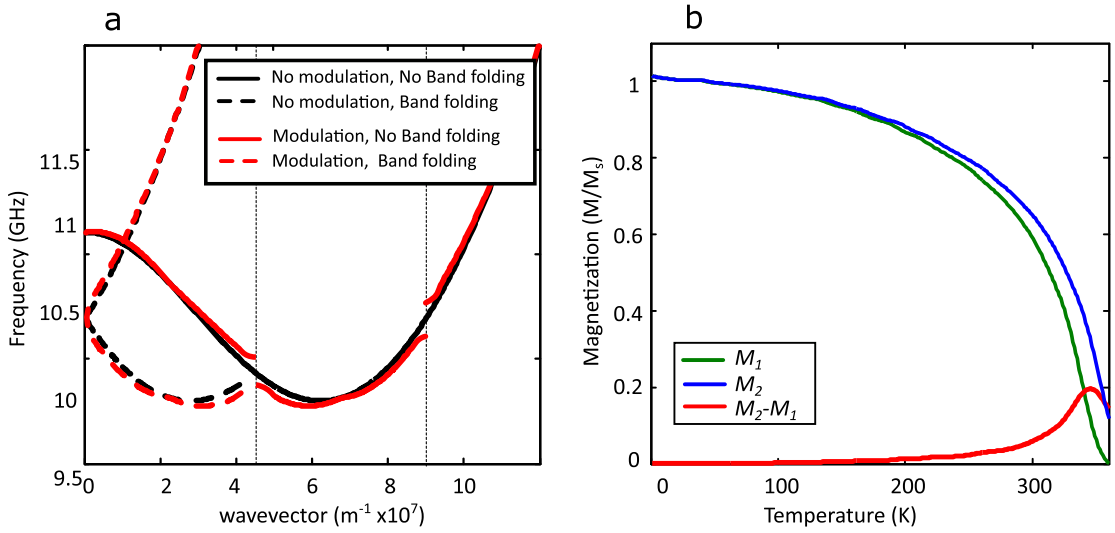

Figure 5. (a) A schematic of the frequency versus the momentum dispersion of the magnonic modes in the lowest backward volume mode for a thin film; black lines correspond to the unperturbed mode and red lines indicate the effect of a magnetic modulation. Dashed lines, both black and red, correspond to the same bands folded into the first Brillioun zone of the magnonic lattice. The used parameters are $\mu_0 H = 0.14$ T, $\mu_0 M = 0.58$ T and a magnetic modulation of 0.018 T. (b) The magnetic potential estimated from measurements shown in figure 4(a) considering an offset of the Curie temperature between the two magnetic phases.

periodicity of the twinned structure:

$$M_{\mathrm{eff}}(T) = M(T) + \sum_{n=1}^{\infty} \gamma_{q_x,n}(T)(M(T - \Delta T) - M(T))\sin(2n\pi x). \quad (2)$$

We then assume that the width of the band gaps induced by the periodic modulation in the Curie temperature is primarily determined by the Fourier component of the effective magnetization, $\gamma_{q_x,n}(T)$, corresponding to the observed mode [11]. We modeled the temperature dependence of the magnitude of the magnetic potential by considering a periodic structure with the sample having two different Curie temperatures: $T_C = 355$ K and $T_C = 370$ K. The corresponding periodic magnetic potential is defined as the difference in magnetization between the magnetization of the two materials, say M_1 and M_2 (see, figure 5(b), which in equation (2) corresponds to $M(T - \Delta T)$ and $M(T)$). This potential thus depends strongly on temperature, increasing abruptly around 250 K in the *type a* sample, explaining the appearance of the split magnonic mode.

The correct estimates of the dispersion relations are given by equation (1) replacing the magnetization M_{eff} with $M_{\pm}$:

$$M_{\pm,n} = M(T) \pm \gamma_{q_x,n}(T)(M(T - \Delta T) - M(T)), \quad (3)$$

where $\gamma_{q_x,n}$ is the nth Fourier component for the magnetization difference between the domain's magnetization, and ΔT is the difference in Curie temperature between the two mentioned magnetization values. The exact amplitudes of the Fourier components of the magnetic potential are unknown unless explicit knowledge of the magnetic structure is known. The Fourier component, $\gamma_{q_x,n}$, thus becomes an unknown fit parameter in our model, which depends on the exact nature of the magnetic potential.

To compare the results from our model with the experimental results, we used values for thickness and domain periodicity obtained through direct x-ray diffraction measurements [13]. The spin stiffness D was approximated by its linear dependence on the magnetization, using measurements presented in [21]. The magnonic band gap was given using $M_{\pm}$ estimated by the difference in magnetization at each temperature (as plotted in figure 5(b)) and scaling it by γ, which is a fitting constant in the model.

We first applied the model calculations to the sample with a smaller thickness ($d = 38$ nm and $\lambda_{\mathrm{twin}} = 48$) and found a good agreement in the temperature dependence for the lower 101 mode and the mode that crosses and hybridizes with the FMR line (see blue and green lines in figure 6(a)). We also performed a calculation using the same model and parameters for the magnetic field dispersive data measured through coplanar wave guides, showing excellent agreement between the data and model at all frequencies and fields (see blue lines in figure 4(b)). We notice here that in general it is found that each mode (e.g. 101) splits up into a bonding (101) and an anti-bonding (101*) configuration, where the bonding mode is much easier to excite.

Applying the same model to the 96 nm thick sample ($\lambda_{\mathrm{twin}} = 71$ nm) (shown in figures 2(c)–(e) and figures 3(a) and (b)) we observe a more complex structure. At low temperatures only the original FMR mode is observed, whereas we also observe 101- and a 202-like excitations as well as the corresponding band gaps when the temperature increases. The 202 mode crosses the original FMR mode in a similar way to the 101 mode in the thinner sample (figure 6(a)).

The fit parameters used in the simulation are listed in table 1. The deviation up to 20% from the integral numbers in the actual mode numbers is as expected, since these parameters accommodate effects like the pinning of the spin waves to the surfaces and other thickness variations in the material, which are not considered in our modeling.

It is enlightening to plot the simple dispersion relations of these modes given by equations (1) and (3) in order to gain further insight into the origin of the modes. Figures 6(d)–(e) show the effect of a modulation potential. The branches plotted in figures 6(a)–(b) correspond to the split states found below and above the calculated modes without in-plane periodic perturbation (black lines in figures 6(d)–(e)).

The nature of the 101 and 202 modes is a two-dimensional closed flux structure. These modes consist of a simultaneous in- and out-of-plane spin standing wave structure with an in-plane periodicity set by the twin-boundary-induced magnetic modulation, and an out-of-plane periodicity set by the thickness of the film. An ordinary one-dimensional mode (e.g. 001) would display a strong in-plane asymmetry. However, due to the mixed mode character, the modes form vortex-like structures that lose most of the in-plane anisotropy found for the pure in-plane FMR modes [25]. The double periodicity of the magnetic modulation compared to the structural periodicity originates from an alternating configuration of the vortex rotation supporting shared domain boundaries. This yields the lowest possible exchange energy while still maintaining low dipole fields; we thus believe that we have observed the lowest energy vortex configuration.

In our fitting procedure, the gap seems to be slightly larger than that estimated from the T_C difference extracted from the FMR data. The used γ_{q_x} is consistent with a higher difference in T_C being $\Delta T \simeq 25$ K instead of 20 K, which still remains within the uncertainty of T_C determination. The difference may, however, be

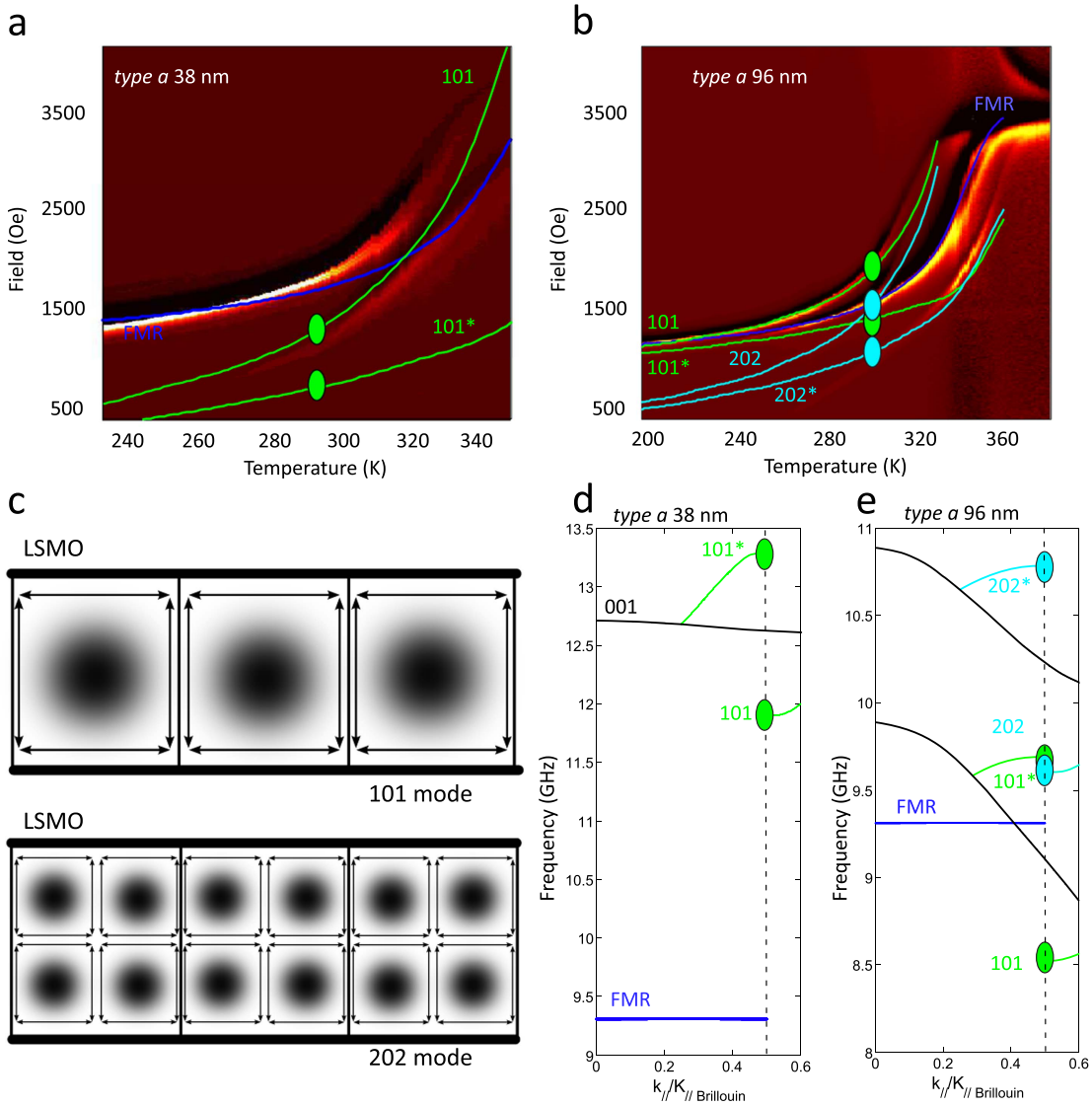

Figure 6. The nature and dispersion relations of magnonic modes. (a) and (b) show the temperature dependence of the 9.37 GHz FMR spectra of a 38 nm thick and 96 nm thick *type a* sample, respectively. The curves corresponding to calculations using equations (1) and (3) and the modulation M_{q_x} described in figure 5(b) are added to the measurements. (c) A schematic plot of the vortex-like states formed by the 101 and 202 modes. The gray shading outlines the antinode structure of the combined modes. The 101^* and 202^* would be shifted relative to the twin boundaries marked by black lines. (d) and (e) are schematic views of the evolution of modes perpendicular to the film at the resonance condition. The evolution of the frequency ($k_{||}$) changes from 0 to the $q_{||}$ (the vector defined by the periodic potential). Thin black lines correspond to the case without any periodic magnetization.

Table 1. Parameters used in the model calculations.

Sample/Line	l	n	$\gamma_{q_x,m}$
Thick type at FMR	—	—	—
Thick (96nm) *type a* 101	1	1.2	2.3
Thick (96 nm) *type a 202*	1.95	2	2.3
Thin (38 nm) *type a 101*	1	0.9	3.5

explained by considering the effects neglected in our model. One possibility is that the periodic modulation of the material magnetization produces an additional demagnetization field with the same periodicity. An additional demagnetization field would contribute more in areas with larger magnetization, and less in other areas. Our modeling was restricted to the first Fourier components of the magnetic potential and thus dismisses information on the spatial distribution of magnetization. More precise modeling can be done [26, 27] when the periodic perturbation of the film's magnetic properties is known.

To summarize, we have reported on how growth-induced periodic structural modulation creates a spatially well-determined magnetic contrast in magnetic thin film. The method forms the basis for the existence of magnonic modes, where the periodic perturbation can be controlled by temperature and growth conditions, resulting in modulations on the length scales of only tenths of nanometers [13]. The combination of low damping magnetic material, the growth control of the strain, and the high dependence of saturation magnetization on the strain is unique in magnetic oxides and offers excellent possibilities for tuning magneto-dynamic properties. These fundamental properties are not *per se* unique to the LSMO system, and may also apply to other magnetic oxides, thus offering a rational route to the bottom-up control of magneto-dynamic modes.

Acknowledgments

The research has been supported by the Research Council of Norway, NANOMAT programme, grant no. 10239707, and the Swedish Foundation for International Cooperation in Research and Higher Education (STINT) for financial support. FM acknowledges support from the Ramón y Cajal program through RYC-2014-16515 from MINECO through the Severo Ochoa Program for Centers of Excellence in R&D (SEV-2015-0496). PN and RM thank the Swedish Research Council (VR) and the Göran Gustafsson Foundation, Sweden, for funding. ADK acknowledges support from NSF-DMR-1610416.

ORCID

Erik Wahlström https://orcid.org/0000-0003-1905-5880
Ferran Macià https://orcid.org/0000-0001-5972-4810
Jos E Boschker https://orcid.org/0000-0001-9122-2079
Roland Mathieu https://orcid.org/0000-0002-5261-2047

References

[1] Neusser S, Botters B and Grundler D 2008 *Phys. Rev.* B **78** 054406
[2] Nikitov S, Tailhades P and Tsai C 2001 *J. Magn. Magn. Mater.* **236** 320
[3] Kruglyak V and Hicken R 2006 *J. Magn. Magn. Mater.* **306** 191
[4] Demokritov S, Sergej O, Slavin A and Andrei N 2013 *Magnonics: from fundamentals to applications* (Berlin: Springer) (https://doi.org/10.1007/978-3-642-30247-3)
[5] Chumak A V, Vasyuchka V I, Serga A A and Hillebrands B 2015 *Nature Phys.* **11** 453
[6] Wang Z K, Zhang V L, Lim S C, Ng H S, Kuok S, Jain M H and Adeyeye A O 2009 *Appl. Phys. Lett.* **94** 083112
[7] Wang Z K, Zhang V L, Lim H S, Ng S C, Kuok M H, Jain S and Adeyeye A O 2010 *ACS Nano* **4** 643
[8] Lenk B, Ulrichs H, Garbs F and Münzenberg M 2011 *Phys. Rep.* **507** 107
[9] Serga A A, Chumak A V and Hillebrands B 2010 *J. Phys. D: Appl. Phys.* **43** 264002
[10] Tacchi S, Madami M, Gubbiotti G, Carlotti G, Tanigawa H, Ono T and Kostylev M P 2010 *Phys. Rev.* B **82** 024401
[11] Tacchi S, Duerr G, Klos J W, Madami M, Neusser S, Gubbiotti G, Carlotti G, Krawczyk M and Grundler D 2012 *Phys. Rev. Lett* **109** 137202
[12] Tacchi S, Montoncello F, Madami M, Gubbiotti G, Carlotti G, Giovannini L, Zivieri R, Nizzoli F, Jain S and Adeyeye A O 2011 *Phys. Rev. Lett.* **107** 127204
[13] Boschker J E, Monsen Å F, Nord M, Mathieu R, Grepstad J K, Holmestad R, Wahlström E and Tybell T 2013 *Philos. Mag.* **93** 1549
[14] Jiang Y, Gao G Y, Wang Y and Chan H L W 2010 *Solid State Commun.* **150** 2028
[15] Soh Y-A, Aeppli G, Mathur N D and Blamire M G 2000 *Phys. Rev.* B **63** 020402
[16] Maurice J L, Pailloux F, Barthelemy A, Rocher A, Durand O, Lyonnet R and Contour J P 2002 *Appl. Surf. Sci.* **188** 176
[17] Maurice J L, Pailloux F, Barthelemy A, Durand O, Imhoff D, Lyonnet R, Rocher A and Contour J P 2003 *Phil. Mag.* **83** 3201
[18] Park J H, Vescovo E, Kim H J, Kwon C, Ramesh R and Venkatesan T 1998 *Nature* **392** 794
[19] Bowen M, Bibes M, Barthelemy A, Contour J P, Anane A, Lemaitre Y and Fert A 2003 *Appl. Phys. Lett.* **82** 233
[20] Jin S, Tiefel T H, McCormack M, Fastnacht R A, Ramesh R and Chen L H 1994 *Science* **264** 413
[21] Golosovsky M, Monod P, Muduli P and Budhani R 2007 *Phys. Rev.* B **76** 184413
[22] Monsen Å, Boschker J E, Macià F, Wells J W, Nordblad P, Kent A D, Mathieu R, Tybell T and Wahlström E 2014 *J. Magn. Magn. Mater.* **369** 197
[23] Flovik V, Macià F, Lendínez S, Hernàndez J M, Hallsteinsen I, Tybell T and Wahlström E 2016 *J. Magn. Magn. Mater.* **420** 280
[24] Gurevich A G and Melkov G A 1996 *Magnetization Oscillations and Waves* (Boca Raton, FL: CRC Press)
[25] Pan H, Zhang V L, Di K and Kuok M H 2013 *Nanoscale Res. Lett.* **8** 115
[26] Gallardo R A, Banholzer A, Wagner K, Körner M, Lenz K, Farle M, Lindner J, Fassbender J and Landeros P 2014 *New J. Phys.* **16** 023015
[27] Körner M, Lenz K, Gallardo R A, Fritzsche M, Mücklich A, Facsko S, Lindner J, Landeros P and Fassbender J 2013 *Phys. Rev.* B **88** 054405